Proceedings of the ASME 2010 3rd Joint US-European Fluids Engineering Summer Meeting and 8th International Conference on Nanochannels, Microchannels, and Minichannels
FEDSM-ICNMM2010
August 1-5, 2010, Montreal, Canada

FEDSM-ICNMM2010-30122

TRANSIENT NUMERICAL COMPUTATION OF THE TEMPERATURE OF ELECTRONIC DEVICES IN PASSENGER CARS

Dr. Florence MICHEL
Daimler AG
Sindelfingen, Germany

Prof. Bernard DESMET
Laboratoire de Mécanique et Energétique
Valenciennes, France

ABSTRACT

In order to ensure a reliable operation of electronic devices in a passenger car, its thermal situation is evaluated in a digital prototype. Of particular interest is to predict the time period, during which the electronic system embedded in the vehicle works within its optimal operating temperature range, in order to compare it with the vehicle specifications. In the present work, iterative coupling simulation strategies and numerical models to predict the temperature of the electronic equipment in a passenger car under time-dependent operating conditions and thermal loads have been developed and validated. The co-simulation strategies are investigated by means of two complex electronic systems embedded in a passenger car. The comparison with experimental results shows that the parallel discrete coupling strategy provides consistent temperature predictions within reasonable computation times in case of coupled problems for which the characteristic time for heat transport by convection is strongly dependent on the simulation time. As for the serial staggered coupling strategy, it is adapted to coupled problems, for which the characteristic time for convection is much smaller than the characteristic time for conduction. To predict the warm-up of an electronic system over several minutes, this strategy provides an efficient model generation and accurate temperature predictions within 1K.

INTRODUCTION

During the development process of a passenger car, the integration of the electronic equipment in the vehicle results from the intervention of different departments. In the department Energy Management of Daimler AG, the temperature of critical electronic devices is evaluated successively at each digital phase of the development process by means of computations of the full vehicle. For multiple reasons such as electronics architecture, user accessibility and assembly facilities for serial production, electronic devices are often grouped by application type and located in small enclosures of the vehicle (Fig. 1). There, the electronic device tends to warm up over the time, which can lead to a drop in its performance, reliability or life expectancy. The present study focuses on two complex electronic systems, on the one hand a lead-acid back battery situated in a spare-wheel cavity under the trunk, on the other hand a sound amplifier assembled in a cavity between the engine compartment and the cabin under the floor covering of the passenger (Fig. 2).

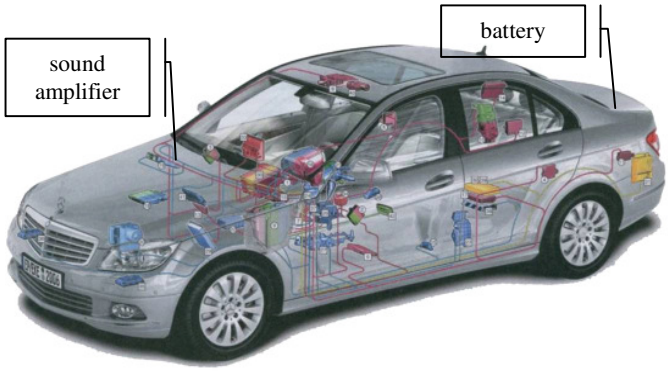

Figure 1. Packaging of the electronic equipment in the Mercedes-Benz C-Class

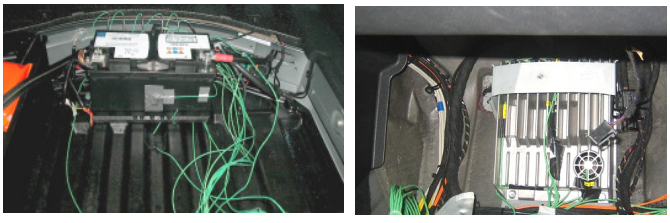

Figure 2. Back battery in the spare-wheel cavity (left) and sound amplifier in the feet compartment (right)

The operating conditions of the car and of the electronic device, also the climatic conditions are settled with a so-called use case. Standard use cases consist of a first phase of pre-conditioning with warming-up, followed by a period of thermal load, e.g. uphill drive with load trailers, completed by thermal soak with engine shut off (Fig. 3). With such a use-case, the spare-wheel cavity is heated from below by the exhaust gas system nearby, which may affect the battery temperature by conduction with its case and by natural convection in the sealed cavity. As for the sound amplifier, it may be warmed up by conduction with the body shell and by mixed convection in the feet compartment slightly opened to the cockpit compartment.

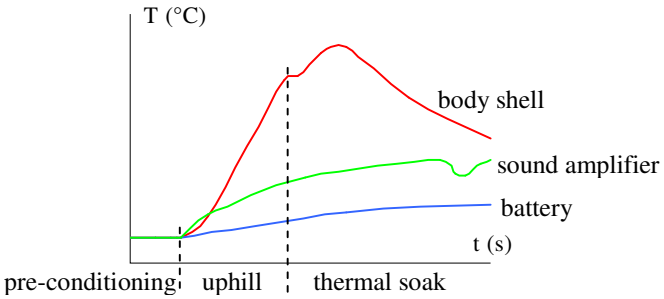

Figure 3. Typical temperature profiles in a vehicle for usual use cases

For the thermal management of a full passenger car, numerical methods have been developed to predict the temperature of the engine compartment and underbody [1, 2]. The main numerical problems encountered, the interaction of the different cooling applications of the vehicle and the coupled heat transfer modes, have been solved using a coupling code strategy [3, 4]. Due to the complexity of the geometry in electronic systems, the heat transfer modes, in particular conduction, have been examined in the literature at one geometric level or time scale [5, 6]. For the thermal management and design of electronic systems, several numerical tools are widely used by electronics suppliers. Nevertheless, their use is limited to design electronic systems in laboratory ambient conditions [7, 8, 9]. Therefore, no numerical method to compute the temperature of electronic systems dealing with complex geometries and environment boundaries has been found in the literature. Furthermore, the methods presented in the literature to solve the coupled heat transfer modes – convection, conduction and radiation – are limited to stationary operating conditions. First, numerical strategies for the computation of the coupled heat transfer modes in electronics compartments must be developed. This is discussed in a first part. Moreover, numerical models for the computation of natural and mixed convection in electronic cavities must be investigated, in particular in view of mesh requirements and turbulence modeling. These models are presented in a second part. Finally, the coupling codes strategies reviewed in a first part are validated in comparison with measurements in the full vehicle, providing the accuracy of the numerical strategies in terms of heat transfer.

NOMENCLATURE

c_p	[J kg^{-1} K^{-1}]	Specific heat capacity
D_H	[m]	Hydraulic diameter
F_{ij}	[-]	View factor from surface i to surface j
Gr	[-]	Grashof number
H	[m]	Generic length, i.e. height
h	[W m^{-2} K^{-1}]	Heat transfer coefficient
k	[W m^{-1} K^{-1}]	Thermal conductivity
L	[m]	Characteristic length
$\dot{q}$	[W m^{-2}]	Heat flux
$\dot{S}$	[W m^{-3}]	Heat rate per unit volume
Ra	[-]	Rayleigh number
Re	[-]	Reynolds number
δt	[s]	Characteristic time
T	[K]	Temperature
u	[m s^{-1}]	Velocity magnitude
u_i,u_j	[m s^{-1}]	Velocity components
y	[m]	Normal distance from the wall to the near-wall cell node
x_i,x_j	[m]	Cartesian coordinates

Greek symbols

ε	[-]	Emissivity (radiation)
μ	[kg m^{-1} s^{-1}]	Dynamic (molecular) viscosity
ν	[m^2 s^{-1}]	Kinematic viscosity
ρ	[kg m^{-3}]	Mass density

Physical constant

$\sigma = 5.67051\times10^{-8}$	[W m^{-2} K^{-4}]	Stefan-Boltzmann's constant

Subscripts and superscripts

c	Coupling
cond	Conduction
conv	Convection
f	Fluid
load	Prescribed from load case
m	Mean
n1	Node of the near-wall cell
rad	Radiation
ref	Reference
s	Solid
t	Turbulent

DEVELOPMENT OF NUMERICAL METHODS

In order to determine the geometric and time scales relevant for the computation of the temperature of the electronic equipment in a passenger car, the characteristic time of temperature propagation by convection and conduction is first estimated.

Characteristic time of temperature propagation

The time scales associated to the heat transfer modes are discussed at two geometric levels: the electronic device and the electronics cavity in the vehicle. The time scales are evaluated with a non-dimensionalization analysis of the transport

equations in the fluid by convection and in the solid by conduction. The resulting characteristic time is representative of the temperature propagation in the fluid at the level of fluid motion and in the solid at the level of temperature gradients. The time scales are investigated on the basis of the back battery and of the sound amplifier. Corresponding characteristic dimensions are shown in Fig. 4.

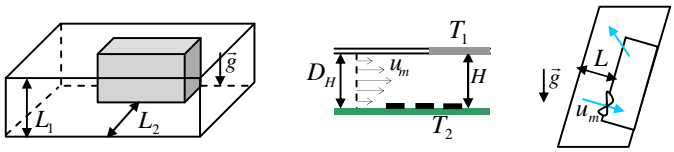

Figure 4. Characteristic dimensions for the back battery (left) and sound amplifier at the device level (middle) or cavity level (right)

Back battery At the end of the pre-conditioning period, the solid temperatures of the cavity have reached a permanent state. Due to the relatively small temperature gradient in the solid at this state, convection in the enclosure approaches the conductivity state with a stratified temperature distribution. Then, during the driving and soak phases, the time-dependent environment temperatures yield to an evolution of the natural convective flow over the simulation time, from oscillating to turbulent regimes, according to the Rayleigh number ranging between $Ra = 9.7\times10^5$ and $Ra = 4.6\times10^7$. Experiments of the literature show that the time period for the flow to reach a full developed state ranges between several minutes for turbulent flows up to several hours for laminar and oscillating flows [10]. It means that, over the testing time period, the flow may never reach a fully developed regime, but evolving between different bifurcations. Over the testing time period, the characteristic time relative to natural convection in the cavity is ranging between:

$$4.4\times10^{-3}\,s \le \delta t = \frac{L^2}{\nu Gr^{1/2}} \le 6.4\times10^{-1}\,s \qquad (1)$$

Moreover, temperature gradients in the body shell of the spare-wheel cavity may occur. The characteristic time relative to conduction in the cavity is provided by:

$$\delta t \le 3.2\times10^{-1}\,s \qquad (2)$$

Sound amplifier During the driving phase, the fan may switch on rapidly and the period of natural convection may be consequently relatively short. With a Rayleigh number of $Ra = 3.4\times10^3$, the natural convective flow in the sound amplifier may be at the onset of the oscillating state [10]. The characteristic time relative to natural convection in the sound amplifier is given by:

$$\delta t = \frac{H^2}{\nu Gr^{1/2}} = 7.5\times10^{-2}\,s \qquad (4)$$

After activation of the fan, the flow state is characterized using the Reynolds number, $\mathrm{Re} = 1.1\times10^3$ and the Grashof number, $Gr = 9.6\times10^6$. In this range, the effect of buoyancy forces is small in comparison with the viscous and inertial forces [11]. The characteristic time in the electronic device derives directly from the prescribed velocity:

$$\delta t = \frac{D_H}{u_m} = 9.3\times10^{-3}\,s \qquad (5)$$

Furthermore, the heat sink of aluminum alloy is submitted to strong temperature gradients in the heat path between the chips and the cool ambient air. The characteristic time relative to conduction in the heat sink is provided by:

$$\delta t = 1.9\,s \qquad (6)$$

In the compartment of the sound amplifier, the strength of buoyancy forces is large enough to reduce the effect of forced convection, as the Reynolds and Grashof numbers are, respectively, $\mathrm{Re} = 4.2\times10^2$ and $Gr = 1.2\times10^6$ [12]. The characteristic time is relative to natural convection in the compartment is:

$$\delta t = \frac{L^2}{\nu Gr^{1/2}} = 0.3s \qquad (7)$$

At the geometric level of the compartment, temperature gradients in the carpeting of the compartment may occur. The characteristic time relative to conduction in the compartment is found of:

$$\delta t \le 425\,s \qquad (8)$$

As a conclusion, multiple characteristic times of heat transfer by convection and conduction have been found depending on the geometric level considered and on the evolution of the flow with the testing time.

Mathematical model

To overcome the problem of multiple characteristic times of heat transfer in electronics cavities, each mode of heat transfer is solved separately. A corresponding mathematical model of governing equations, boundary conditions and initial conditions is described in the following. Moreover, a transient coupling method is required to ensure the equality of heat fluxes and temperatures at the interface between fluid and solid. It will be discussed in the last part.

Conduction in the solid To determine the temperature of the electronic equipment running under transient operating conditions and thermal loads, the energy equation is solved in the solid region. Diffusive conduction at a macroscopic level only is considered with the extended Fourier equation.

With $\dot{S}_{load}$ the prescribed heat rate per unit volume, it is provided by:

$$\rho(T)c_p(T)\frac{\partial T_s}{\partial t} - div\left([k(T)]\overrightarrow{grad}(T_s)\right) = \dot{S}_{load} \qquad (9)$$

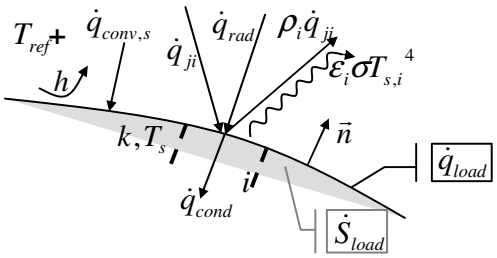

Figure 5. Heat fluxes at the fluid-solid interface

Coupling condition at the interface At the interface fluid-solid, the convective and radiation heat fluxes are given as boundary conditions at each time-step. With $\vec{n}$ the vector normal to the surface as illustrated in Fig. 5, the Neumann boundary condition at the interface fluid-solid is provided by:

$$[n]^T \cdot [k(T)]\overrightarrow{grad}(T_s) - \dot{q}_{conv,s} = \dot{q}_{rad} + \dot{q}_{load} \qquad (10)$$

Radiation The radiation heat flux is obtained by solving the system composed of equations 11 and 12:

$$\dot{q}_{ji} = \sum_j \dot{q}_j F_{ji} = \sum_j (\varepsilon_j \sigma T_j^4 + \rho_j \dot{q}_{ij}) F_{ji} \qquad (11)$$

$$\dot{q}_{rad} = \varepsilon_i \dot{q}_{ji} - \varepsilon_i \sigma T_i^4 \qquad (12)$$

Convection in the fluid For reasonable computing times in the development process, the flow in electronic cavities is computed with a steady-state approach. The range of validity of the steady-state approach for the computation of buoyancy-driven flows has been investigated in rectangular and cubical cavities for a large range of Rayleigh number covering laminar, oscillating and turbulent regimes [13]. The investigation is discussed in a companion paper [14]. Moreover, for high temperature differences in electronic devices up to 60K, the physical properties of the fluid are dependent on temperature. Therefore, a continuous flow of a Newtonian expansible gas is assumed in electronic compartments. To model the turbulent flow, the conservation equations are written with the Reynolds decomposed variables using the Favre averaging and time-averaged, providing the RANS (Reynolds averaged Navier-Stokes) equations. The turbulent heat flux is provided by the sum of two terms $\overline{\dot{q}_j} + \overline{\dot{q}_{j,\mathrm{Re}}}$ with:

$$\overline{\dot{q}_j} = k\frac{\partial \overline{\overline{T_f}}}{\partial x_j} \qquad (13)$$

$$\overline{\dot{q}_{j,\mathrm{Re}}} = -\overline{\rho} c_p \overline{\overline{u_j'' T_f''}} \qquad (14)$$

Initial conditions As the standard use cases to test the temperature of the electronic equipment in a vehicle are based on a first phase of pre-conditioning of several hours, the solid temperature is assumed initially homogeneous and the fluid isothermal and at rest.

Solid and flow solvers

In this work, different solvers are used for the computation of the conduction, radiation or convection heat transfer mode. Conduction and radiation have been solved either with the thermal analysis software RadTherm [15] or with the finite element code PERMAS [16] combined with the radiation code POSRAD [17]. Furthermore, the commercial finite-volume CFD code STAR-CD [17] has been used to solve the flow.

Thermal analysis software RadTherm It performs heat transfer analysis for the temperature prediction of thin walls. Each element of the thin wall shows two surfaces (front and back) separated by a specified thickness. A thermal node is associated with each surface, as shown in Fig. 6.

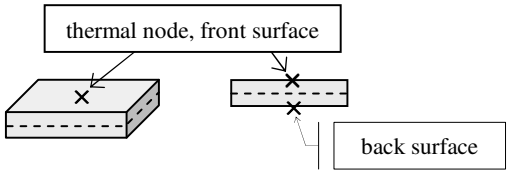

Figure 6. Isometric view (left) and section (right) of an element in RadTherm.

For practical reasons, triangle elements are used in this work to mesh the surfaces. The energy balance is calculated at each thermal node. RadTherm possess its own radiation solver; the view factors are calculated using a single plane variant of the hemi-cube method. The transient energy equation and the radiation enclosure equation are discretized using the Crank-Nicholson implicit finite difference scheme, unconditionally stable and second-order accurate in time and space. Then, the iterative SOR (successive over-relaxation) method is used in conjunction with a secondary direct method (Gauss elimination with partial pivoting) to solve the discretized equations.

Finite element code PERMAS and radiation code POSRAD The energy balance is computed by analogy with structural mechanics. The energy equation is solved in 3D tetrahedral solid finite elements. Moreover, the boundary condition at the fluid-solid interface is solved in 2D triangle membrane elements, associated with the solid elements. The governing equations 9 and 10 are discretized following the Galerkin procedure and using constitutive matrices by analogy with structural mechanics. Accordingly, the system of matrices is solved with the iterative Newton-Raphson method. For the

computation of the view factors, POSRAD works with the discrete beam method [17].

Finite-volume CFD code STAR-CD To mesh the complex geometries with shaped and curved surfaces encountered in electronic enclosures, trimmed meshes are used in this work. They are based on hexahedral cells with trimmed type polyhedral near the subsurface. Moreover, for reasonable computing times in the development process eddy viscosity models are used to close the system composed of the three RANS equations. Any of these models is based on the eddy conductivity concept, for which the turbulent heat flux follows a similar law as the Fourier law for diffusive conduction. It assumes the simple gradient diffusion hypothesis (SGDH). With σ_t the turbulent Prandtl number:

$$\overline{\rho} c_p \overline{\overline{u_j'' T_f''}} = -\frac{\mu_t c_p}{\sigma_t} \frac{\partial \overline{\overline{T_f}}}{\partial x_j} = -k_t \frac{\partial \overline{\overline{T_f}}}{\partial x_j} \tag{15}$$

In STAR-CD, the evaluation of the convective heat transfer is based on the temperature of the first near-wall cell, as illustrated in Fig. 7.

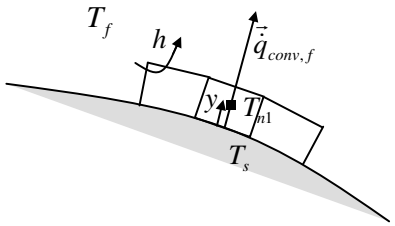

Figure 7. Convective heat flux at the fluid-solid interface.

With y the normal distance from the wall to the near-wall cell node, the convective heat flux at the interface is approximated by STAR-CD by:

$$\dot{q}_{conv,f} = k \frac{T_s - T_{n1}}{y} \tag{16}$$

The governing equations of mass, momentum and energy conservation are discretized by the finite volume (FV) method, which is conservative for connected cell faces. The second-order accurate differencing schemes MARS (monotone advection and reconstruction scheme) for the convective fluxes and the turbulent quantities and CD (central differencing) for the density are used in this work with blending factors of 0.5 and 0.01 respectively. The coupling between velocity and pressure fields is solved using the segregated solution algorithm SIMPLE (semi-implicit method for pressure linked equations).

Mesh mapping The boundary and initial conditions are given on each surface element of the solid solver (PERMAS or RadTherm) and on each volume element of the fluid solver (STAR-CD). Typically, the meshes of both solvers differ in element type, element size and node location, which is referred as non-matching grids, as for example shown in Fig. 8. For data exchange between the two non-matching grids, the mesh mapping tool MpCCI [18] is used. With corresponding nodes between the two non-matching grids, the process of data exchange allows a conservative transfer. This process may not be conservative anymore with orphan nodes, for which partner nodes in both grids are not found.

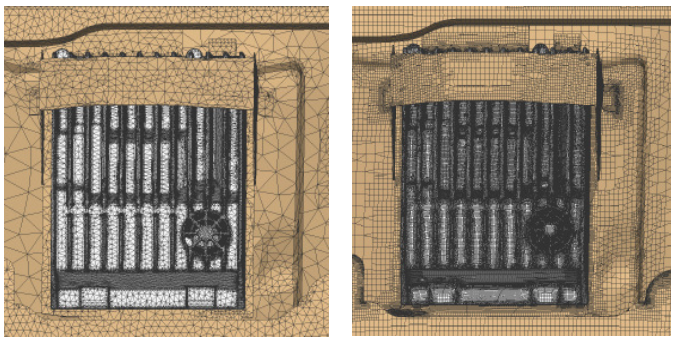

Figure 8. Non-matching grids for computation with PERMAS (left) and STAR-CD (right).

VALIDATION OF CO-SIMULATION STRATEGIES

In order to ensure a correct time-dependent fluid-solid interaction, different coupling codes strategies are investigated, in particular examining the method and frequency of the heat transfer coupling.

Coupling codes strategies

Different approaches are used in this work, a parallel discrete coupling and an iterative serial coupling.

Parallel discrete coupling A first transient thermal analysis with RadTherm is carried out from the stable initial state of the pre-conditioning period. Then, the convective heat transfer mode is evaluated at selected time-steps t^{n_i} and coupled back for a transient thermal analysis, as shown in Fig. 9. An estimation of the convective heat transfer between the coupled time-steps is provided by linear interpolation. The convergence criterion for the co-simulation is the equivalence of the solid temperatures between two consecutive iterations.

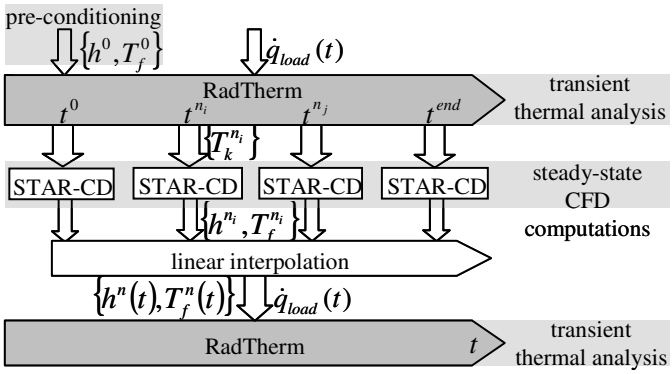

Figure 9. Parallel discrete coupling strategy.

The advantage of this strategy is that it provides reasonable computing times. However, the flow is initially considered isothermal and at rest at each flow computation, but not depending on the flow structure at the previous solid time-step. Moreover, the heat balance at a certain time-step does not rely on the coupling at a previous time-step and the conjugate heat-transfer problem can be reproduced only partially by this strategy. This co-simulation strategy is adapted to coupled problems, for which the characteristic time for heat transport by convection is strongly dependent on the simulation time. Consequently, the validity of this strategy will be verified on the case of the lead-acid battery in a spare-wheel cavity.

Serial staggered coupling The pre-conditioning phase is computed with STAR-CD, which corresponds to the permanent state. The resulting convective heat flux provides the initial conditions necessary to solve the solid. The natural approach for the iterative coupling is a sequential process, in which the flow is solved steady-state between two consecutive time-steps of the solid computation (Fig. 10). The coupling time-steps are user-defined and constant. The solid time-steps are prescribed by PERMAS depending on convergence results and are adjusted to fit the coupling time-steps. In this case also, the co-simulation has converged when the solid temperatures between two consecutive iterations are found equivalent.

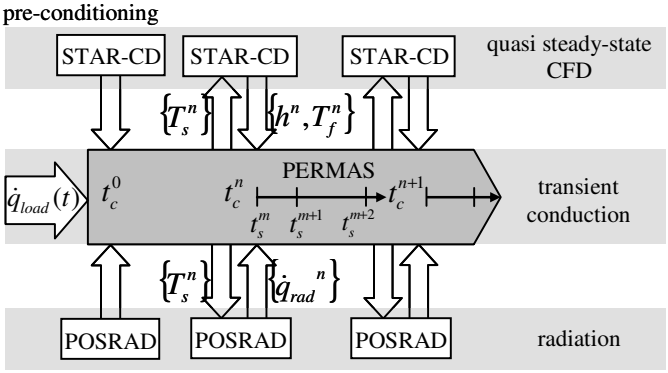

Figure 10. Serial staggered coupling strategy.

For small coupling time-steps that are closed to the solid time-steps, it is assumed that the flow state does not change drastically between two consecutive coupling time-steps. At a certain time-step, the heat flux balance in the solid takes into account the coupling fluid-solid at the previous time-step. The coupling strategy is therefore more accurate for solid temperature predictions than the previous one. It is also more time-consuming due to the numerous CFD computations and mesh mapping operations. As the flow computations provide an iterative evaluation of the convective heat flux, this co-simulation is reasonable in coupled problems, for which the characteristic time for convection is much smaller than the characteristic time for conduction. Therefore, this strategy will be validated on the case of the sound amplifier in a compartment under the passenger's feet.

Procedural method for validation

In the following, the range of validity of the co-simulation strategies proposed is examined on the basis of the back battery and of the sound amplifier. Local temperatures measured with K-type thermocouples are used for the validation of the strategies. In all cases, the error range of the measurement of $\pm 1.5K$ is not represented in the figures.

The procedural method used in the following is divided into two steps:

1. Model parameterization

In order to build a numerical model of the electronic system from the real device in the vehicle, a parameterization of the model is carried out in a first step. Here, the sensitivity of solver parameters is also examined. For reasonable convection boundary conditions during parameterization, the convection heat flux is modeled using a time-dependent punctual distribution of the film temperature measured previously and a constant heat transfer coefficient.

2. Validation of the coupling strategy

Once validated, the numerical models of the lead-acid battery and sound amplifier can be used for the validation of the co-simulation strategies, disposing of flow computations with STAR-CD for the prediction of the convective heat transfer.

Back battery in the spare-wheel cavity

The battery considered is composed of six serial mounted cells, containing plates of lead metal (anode) and lead dioxide (cathode) with an insulating material in between (separator). The plates are submersed in an electrolyte composed of sulfuric acid and water. The difference of charge between the plates leads to an electric current. Regarding critical operating conditions, the temperature of the battery cells should reach as soon as possible 0°C for a satisfying performance and must not exceed 60°C to prevent from failure.

Use cases of winter and summer The use case defined to test the performance of the battery consists of engine cranking followed by idle with battery charge during two hours. The heat generated by charging depends on the SOC (state of charge) of the battery and on the ambient temperature. Ambient temperatures of -10°C and 25°C are prescribed to simulate use cases of winter and summer respectively. In the case of winter, the vehicle is situated in a climatic chamber maintained at constant ambient temperature, while it is located outdoors with sun radiation exposure in the case of summer. In both cases, the vehicle has been pre-conditioned during several hours with the same experimental conditions. The SOC of the battery at the beginning of the experiment is of 70% in case of winter and 50% in case of summer. The experimental set-up can be seen in Fig. 2. The position of the thermocouples in the spare-wheel cavity is shown in annex, Fig. A.1.

Numerical models The model for the thermal analysis with RadTherm is constituted of the battery in the spare-wheel cavity surrounded by the exhaust-gas system, as illustrated in Fig. 11.

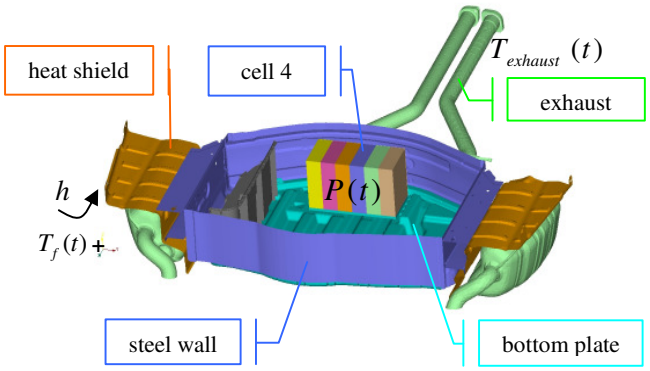

Figure 11. Numerical model for thermal analysis of the battery with RadTherm.

The inner battery is modeled using a main part of lead sulfate considered as a solid of homogeneous temperature in contact with sulfuric acid. The chemical cell is isolated on the upper part with an air layer. The time-dependent electrical heat generated by the battery is imposed on each battery cell. Moreover, the time-dependent temperature of the exhaust-gas system is given as boundary condition. The final surface mesh consists of 160,000 elements. For the computation of the buoyancy-driven air flow in the spare-wheel cavity with STAR-CD, a grid with 12 cell layers in the near-wall region is used (Fig. A.2). The corresponding volume mesh contains three million cells. In the range of Rayleigh numbers considered, the standard low-Re k-ε model is used in the present study.

Sensitivity of solver parameters Transient analyses are carried out with time-steps of 120s, 60s, 30s and convergence criteria of 0.05K, 0.01K and 0.002K. Small discrepancies within 0.1K with experimental results are obtained for a convergence criterion of 0.05K and a time-step of 120s. Consequently, a convergence criterion and time-step of 0.01K and 60s are used for further computations with RadTherm.

Model parameterization Experimental and numerical results for the temperature of the battery cell four and battery casing are presented in Fig. 12. Overall, the numerical model of the battery provides consistent transient predictions of the battery temperature in comparison with measurements for both cases of winter and summer. An improvement in case of summer is expected with the computation of the heat flux distribution with STAR-CD.

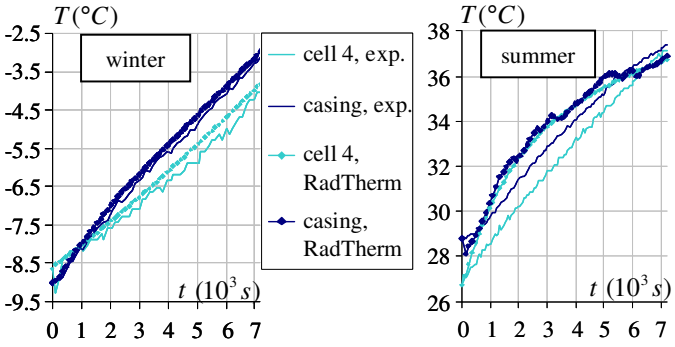

Figure 12. Transient temperature of the battery casing and cell 4; comparison between experimental and numerical results.

Validation of the coupling codes strategy The validity of the parallel discrete coupling process is investigated for the case of summer only. Initially, a transient thermal analysis is carried out with RadTherm. The convective heat transfer in the spare-wheel cavity is modeled, in a first approach, using a fluid part of homogeneous temperature and a constant heat transfer coefficient of 3W/m²K. Four relevant time steps are selected at which the wall temperature distribution computed by RadTherm is sent to STAR-CD: 0s, 780s, 3600s and 7200s. The flow is initially considered isothermal and at rest for each new computation. The temperature distribution and streamlines in the spare-wheel cavity resulting from steady-state flow computations with STAR-CD are shown in annex, Fig. A.3. Between $t = 0s$ and $t = 3600s$ the flow in the cavity is evolving a lot: rolls are first developing longitudinally in the cavity, then reorient themselves in different directions according to temperature gradients. The heat transfer coefficient and film temperature computed by STAR-CD are sent to RadTherm for a second transient thermal analysis. The battery temperature computed by the co-simulation is compared with the experimental results and the predictions of the initial thermal analysis based on a constant convective heat transfer coefficient (Fig. 13).

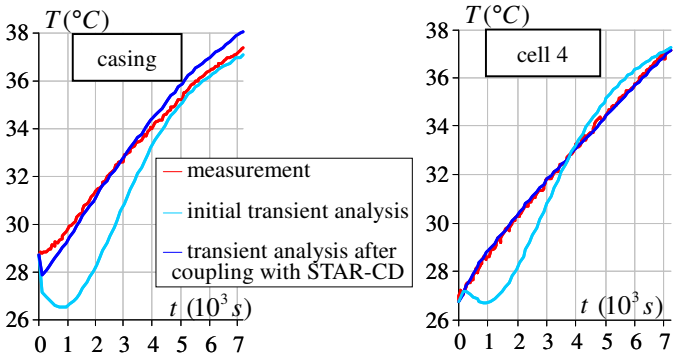

Figure 13. Transient temperature of the battery casing and cell 4; comparison between measurements, initial transient analysis and transient analysis after coupling with STAR-CD.

The battery cell temperature predicted by the co-simulation is lying superimposed with the experimental result. Because of the initial inhomogeneous temperature field initially, the fluid part used to model the convective heat transfer in the cavity for the initial thermal analysis is cooling down during the first ten minutes, which yields to a similar cooling of the battery case and cell. With the flow computations at $t = 0s$ and $t = 780s$ with STAR-CD, the fluid temperature in the spare-wheel cavity is corrected, providing a reasonable prediction for the temperature of the battery case after coupling within 1K.

Sound amplifier in the feet compartment

The sound amplifier is constituted of one populated PCB, which is screwed between a heat sink of aluminum alloy and a steel bottom plate. Among the different electronic modules mounted on the PCB, the FOT (Fiber Optical Transceiver) is the most thermal sensitive. If the ambient operating temperature of the FOT reaches its critical value, the FOT is switched off, which results in a failure of the infotainment bus system. To amplify the low-power signals to a level suitable for driving loudspeakers, most of the heat is generated by five MOSFET (Metal–Oxide–Semiconductor Field-Effect Transistor) power transistors and conducted to the heat sink with thermal grease. Heat conduction in the PCB is limited by a thick trace layer in the laminate substrate. In the following, only the first phase of warm-up before the fan switches on is investigated.

Use case To reach high thermal loads of the engine, the use case consists of a drive period uphill followed by soak. The vehicle is situated in a climatic chamber warmed up at a constant environment temperature and radiation exposure with several hours pre-conditioning. The pre-conditioning and measurement phases are carried out with roof and windows opened, to provide critical thermal conditions in the cabin. The radio is turned on at $t = 300$ s. after the measurements started, corresponding to the beginning of the operation of the sound amplifier. The sound amplifier operates under critical conditions with maximum sound level, maximum bass and treble and IEC noise according to the standards. The experimental set-up can be seen in Fig. 2. The position of the thermocouples in the feet compartment is shown in annex, Fig. B.1 and Fig. B.2.

Numerical models The numerical model for the computation of the conduction and radiation heat transfer modes with PERMAS and POSRAD is restricted to the cavity of the sound amplifier encompassed by the steel cowl on one side and the feet plate and carpeting on the other side, as illustrated in Fig. 14. The numerical model is completely sealed in place of the vent with the cockpit. Heat conduction from the junction of the power transistors to the heat sink can be represented by a 1D network model involving thermal resistance and capacitance (Fig. 15). In the PERMAS model, this heat path is modeled using a resistor consisting of a copper solid layer, which thermal properties are calculated based on the network model.

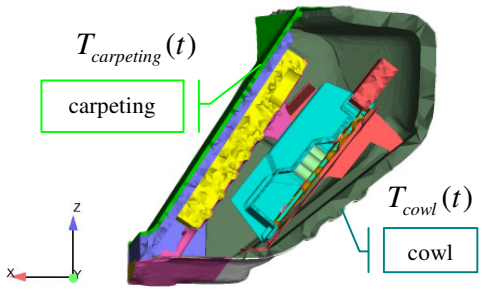

Figure 14. Numerical model for the computation of conduction and radiation with PERMAS/POSRAD in the feet compartment.

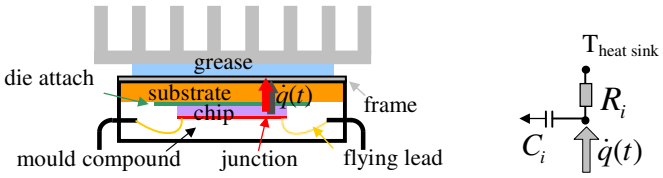

Figure 15. 1D network model for conduction between power transistor and heat sink.

The time-dependent temperatures of the cowl and of the upper carpeting layer are given as boundary conditions. The heat generated by the junction of the power transistors and semiconductors is imposed on the surfaces between both resistors, given as a step function for $t = 300s$. The final mesh consists of 1.37×10^6 solid elements for conduction and 3×10^5 membrane elements for radiation. For the computation of natural convection in the compartment, a boundary layer with 3 layers in the near-wall region of the fins and 9 layers elsewhere is generated. The final volume mesh contains five million cells. In the range of Rayleigh numbers considered, the standard low-Re k-ε model is adopted.

Sensitivity of solver parameters Several coupled simulations are carried out with coupling time-steps of 15s and 30s, for which the flow is computed using 20 or 100 iterations. For the convergence of the residuals in the flow computation, 100 iterations are required. Moreover, as the numerical results with coupling time-steps of 15s and 30s are very similar, coupling time-steps of 30s are used in further co-simulations.

Model parameterization The comparison between experimental and numerical results for the temperature of the FOT, of the fin and bottom plate can be seen on Fig. 16. The temperatures are shown as the difference between the transient temperature and the initial temperature.

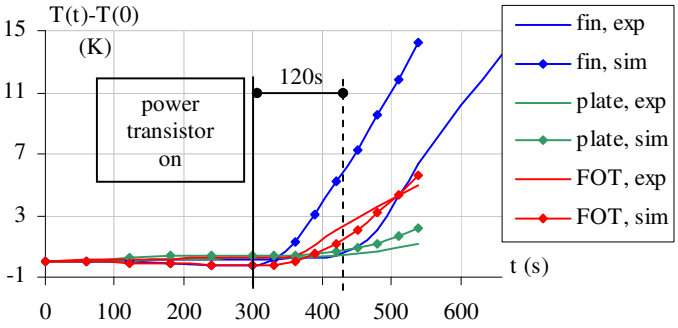

Figure 16. Relative temperatures in the sound amplifier. Measurements and computation PERMAS/POSRAD.

A good agreement is obtained for the temperatures of the bottom plate and FOT. However, the co-simulation predicts the beginning of the warm-up of the fin much before the measurements do. In this case, the thermal response has been measured in the vehicle 120s after music on. For verification, the distribution of the surface temperature of the heat sink has been measured with a thermographic camera. Experimental and numerical results at corresponding time can be seen in annex, Fig. B.3. Both distributions are found very similar, showing the warm-up of the heat sink in the region of the power transistors. Moreover, the temperatures of the fin above a transistor over the first seconds of measurement can be seen in Fig. 17.

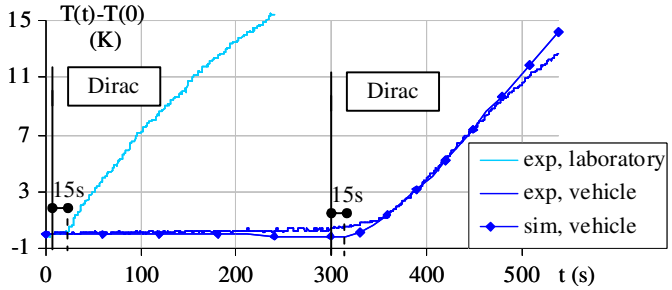

Figure 17. Relative temperatures of the fin for laboratory conditions and operating conditions in the vehicle.

The fin tip starts warming-up 15s after Dirac excitation in the transistors. Assuming the same thermal response in the vehicle, a good agreement between numerical and experimental results in the vehicle is achieved. The incorrect response time of the fin tip measured in the vehicle is attributed to an insufficient contact between the K-type thermocouple and the surface of the fin.

Effect of radiation The heat sink temperature computed with PERMAS/POSRAD in comparison with PERMAS differs only by 0.5K. Therefore, the radiative heat transfer has no considerable effect on the sound amplifier temperature. This can be explained with the moderate temperatures in the enclosure.

Validation of the coupling codes strategy

The streamlines in the cavity of the sound amplifier computed with STAR-CD and the wall temperatures computed with PERMAS at different time-steps can be seen in annex, Fig. B.4. At $t = 420$ s and $t = 540$ s, the amplifier warms up at the base of the fins in the region of the transistors. The temperatures in the amplifier computed by the co-simulation PERMAS/STAR-CD can be seen in Fig. 18 in comparison with the measurements. The slight increase of the overall temperature before the amplifier turns on is well predicted by the co-simulation. The flow computation with STAR-CD accounts for the air recirculation in the cavity, which warms up at the contact with the feet plate and leads to a temperature increase of the amplifier. Overall, the co-simulation between PERMAS and STAR-CD provides a very good agreement between numerical and experimental results, except for a short time period before the fan switches on due to the inaccurate temperature of the carpeting given as boundary condition.

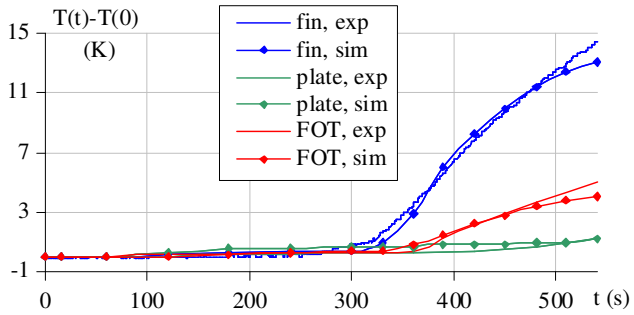

Figure 18. Relative temperatures in the sound amplifier. Measurements and computation PERMAS/STAR-CD.

CONCLUSIONS

To solve the multi-scale coupled heat transfer problem, iterative co-simulation methods have been proposed, which use adapted codes for the prediction of each heat transfer mode. Moreover, a steady-state approach is used to solve the flow. The co-simulation strategies have been validated in comparison with experimental results for two complex electronic systems – a back battery and a sound amplifier – in their real environment of a vehicle. The efficiency and the reliability of both co-simulation strategies have been appraised for implementation in the digital development process. The parallel discrete coupling strategy requires manual mesh mapping, which is relatively time consuming if numerous data exchanges must be performed. Moreover, the prediction of the convective heat flux over time relies highly on the time-steps selected for the coupling. With adapted coupling time-steps, the co-simulation with RadTherm provided consistent temperature predictions of the battery for a long simulation time of several hours within a reasonable total computing time. As for the serial staggered coupling strategy, the small coupling time-steps required for a quasi steady-state computation of the flow imply numerous mesh mapping

processes, which are carried out automatically. These processes yield to unaffordable computing times in the development process for large models of several million elements or for several hours of simulation time.

Moreover, the investigation of the sound amplifier has shown that the computational results are strongly affected by the flow and temperature boundary conditions assigned. To improve the accuracy of the temperature predictions, it is therefore essential to extend the geometrical limits of the computed system as far as possible up to the vehicle scale. Considering the freeze deadlines in the development process which tend to shorten in the next years, the total computing time must be reduced. For more efficient mesh mapping processes, identical mesh surfaces for conduction and convection will be used in the future. Furthermore, to predict the temperature of the electronic system at a chip level, which is affected at the vehicle level by convection, conduction and radiation, the whole system will be decoupled into multiple quasi-closed systems with common boundary conditions to close them properly. An efficient computational method will require a parallel computation of these systems.

ACKNOWLEDGMENTS

This research was funded by Daimler AG, department EP/SAE. The authors would like to thank Prof. Thomas Breitling and Dr.-Ing. Raimund Siegert for supporting and approving the publication of the present work.

REFERENCES

[1] Bauer, W., Ehrenreich, H., Reister, H., 1995, "Design of cooling systems with computer simulation and underhood flow analysis using CFD", Paper No. C496/042, VTMS 2, IMechE, London.

[2] Schuster, M., 2003, "Application of CFD as an efficient analysis tool supporting the experimental investigation of underhood vehicle flows", Paper No. C599/056/2003, VTMS 6, SAE.

[3] Bendell, E., 2005, "Investigation of a coupled CFD and thermal modelling methodology for prediction of vehicle underbody temperatures", Paper No. 2005-01-2044, SAE Papers VTMS 7, Toronto.

[4] Weidmann, E.P., Wiedemann, J., Binner, T., Reister, H., 2007, "Experimental and numerical investigations of thermal soak", J. Wiedemann, Progress in Vehicle Aerodynamics and Thermal Management V, Expert-Verlag, ISBN 978-3-8169-2771-6.

[5] Cheng, H.C., Chen, W.H., Cheng, H.F., 2008, "Theoretical and experimental characterization of heat dissipation in a board-level microelectronic component", Applied Thermal Engrg. 28, pp. 575-588.

[6] Teertstra, P., Yovanovich, M.M., Culham, J.R., 2004, "Modeling of natural convection in electronic enclosures", Inter Society Conference on Thermal Phenomena, pp. 140-149.

[7] Kowalski, T., Radmehr, A., 2000, "Thermal analysis of an electronics enclosure: Coupling flow network modeling (FNM) and computational fluid dynamics (CFD)", Sixteenth IEEE SEMI-THERMTM Symposium, IEEE, pp. 60-67.

[8] Zhao, Z., 2003, "Thermal design of a broadband communication system with detailed modeling of TBGA packages", Microelectronics Reliability, Vol. 43, pp. 785-793.

[9] Eveloy, V., Rodgers, P., Hashmi, M.S.J., 2004, "Application of numerical analysis to the optimisation of electronic component reliability screening and assembly processes", J. Materials Processing Technology, Vol. 155-156, pp. 1788-1796.

[10] Kirchartz, K.R., Oertel, H., 1988, "Three-dimensional thermal cellular convection in rectangular boxes", J. Fluid Mech., Vol. 192, pp. 249-286.

[11] Maughan, J.R., Incropera, F.P., 1987, "Experiments on mixed convection heat transfer for airflow in a horizontal and inclined channel", Int. J. Heat Mass Transfer, Vol. 30, No. 7, pp. 1307-1318.

[12] Mahaney, H.V., Incropera, F.P., Ramadhyani, S., 1990, "Comparison of predicted and measured mixed convection heat transfer from an array of discrete sources in a horizontal rectangular channel", Int. J. Heat Mass Transfer, Vol. 33, No. 6, pp. 1233-1245.

[13] Michel, F., 2009, "Transient numerical computation of the temperature of the electronic equipment in passenger cars", Ph.D. thesis, ED072 – Univ. Lille Nord-de-France.

[14] Michel, F., Desmet, B., 2010, "Transient numerical computation of the temperature of electronic devices in passenger cars: Flow simulation in electronic cavities", Paper No. 30255, 3rd Joint US-European Fluids Engineering Summer Meeting, ASME, Montréal.

[15] Thermoanalytics Inc.: RadTherm Technical Documentation, 2001, Calumet.

[16] Intes GmbH: Permas User Manual, 2004, Stuttgart.

[17] CD-Adapco Group, Methodology and User Guide, Computational Dynamics STAR-CD, Version 3.20, 2004, London.

[18] SCAI Fraunhofer: MpCCI 3.0 – Dokumentation, 2006.

ANNEX A

BATTERY IN THE SPARE-WHEEL CAVITY

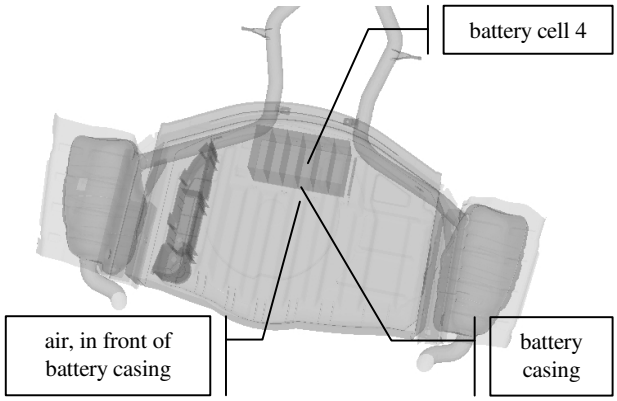

Figure A.1. Position of the thermocouples in the spare-wheel cavity; view from above.

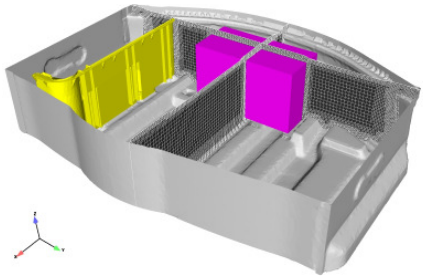

Figure A.2. Mesh used for the computation of the convection heat transfer mode with STAR-CD.

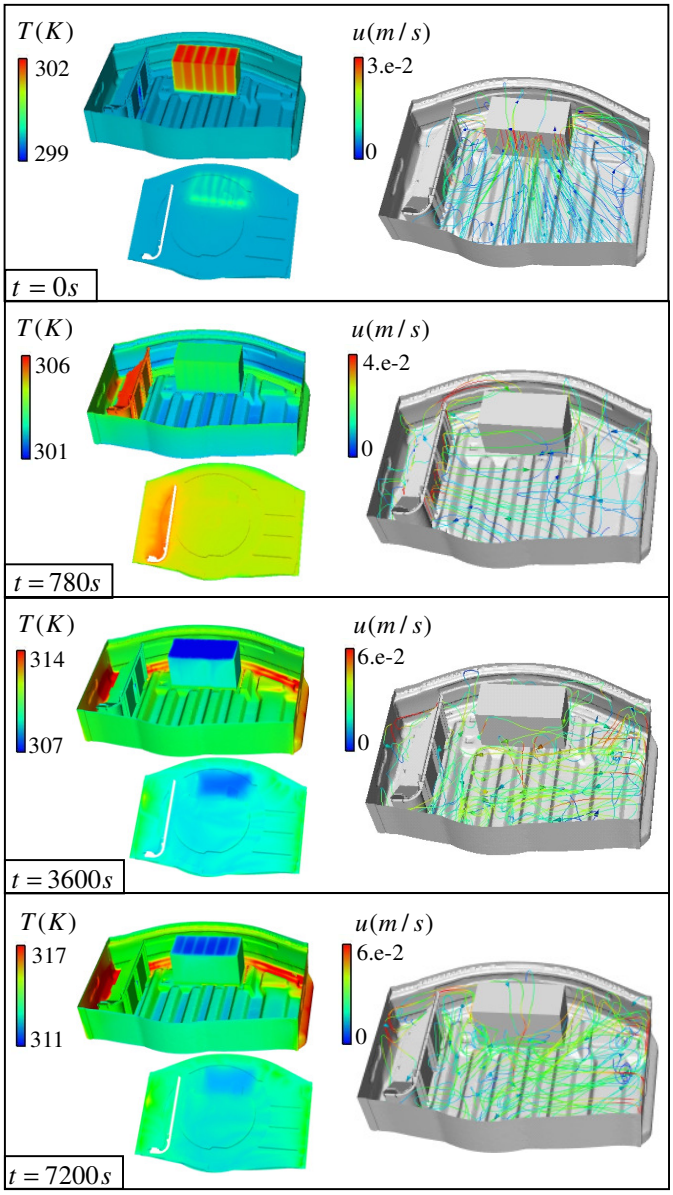

Figure A.3. Temperature distribution (left) and streamlines (right) computed with STAR-CD, case of summer.

ANNEX B

SOUND AMPLIFIER IN THE FEET COMPARTMENT

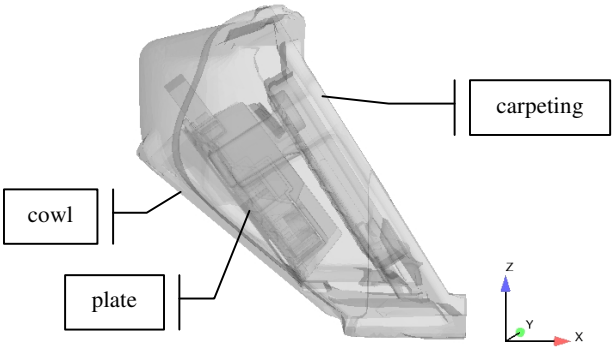

Figure B.1. Position of the thermocouples in the cavity of the sound amplifier; lateral view.

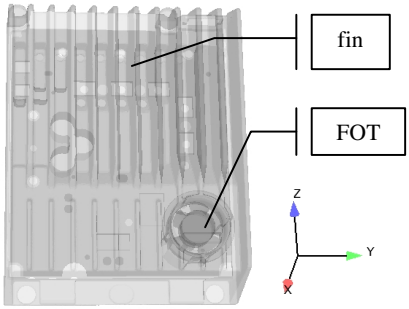

Figure B.2. Position of the thermocouples on the sound amplifier; front view.

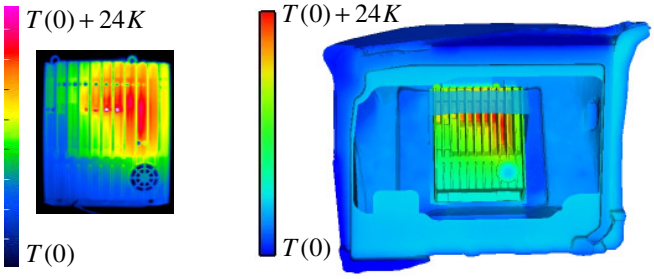

Figure B.3. Surface temperature of the heat sink at $t = 540s$ from measurement (left) and co-simulation PERMAS/POSRAD (right).

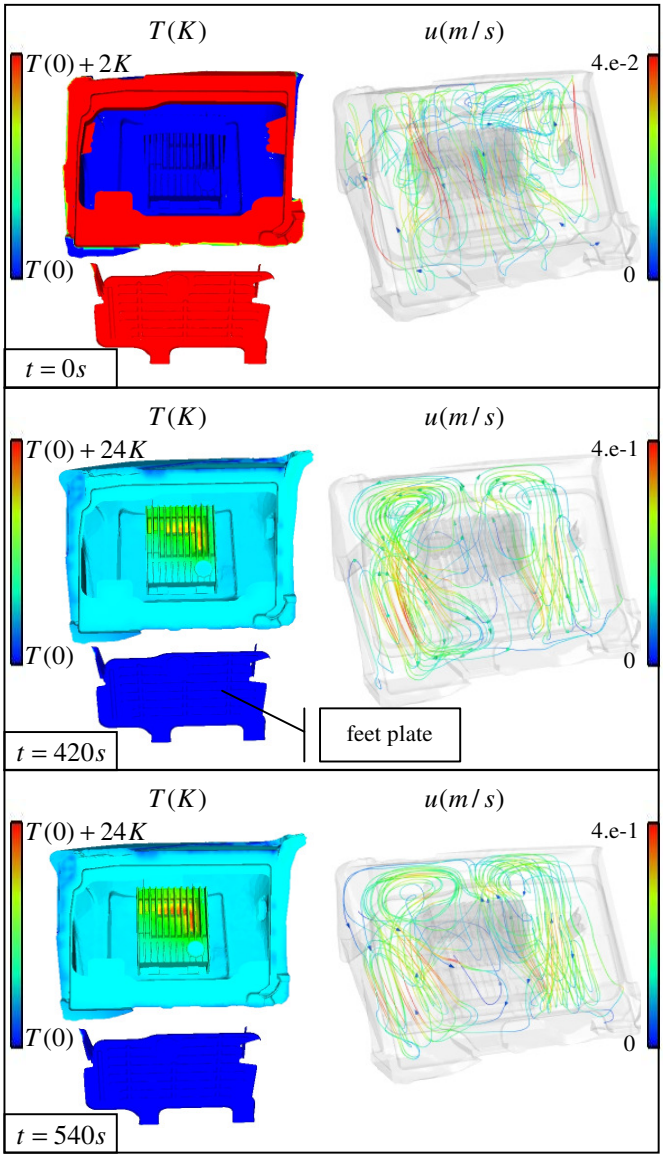

Figure B.4. Temperature distribution predicted by PERMAS/STAR-CD (left) and streamlines by STAR-CD (right).